Tenth International Conference on Computational Fluid Dynamics (ICCFD10), Barcelona, Spain, July 9-13, 2018

ICCFD10-220

Analytical Multidimensional Integration of Heaviside Function for Interface Tracking

Tameo Nakanishi*
Corresponding author: tameo@yz.yamagata-u.ac.jp

* Yamagata University, Japan

Abstract: We propose a novel method for interface tracking using multidimensional Heaviside function. The integrations of the multidimensional Heaviside function over the grid cell and the upwind region to determine the volume fluxes are carried out analytically and explicitly. The new method bears all the benefits of the PLIC type method but does not involve geometric reconstructions of the interface. The new method is simple and efficient, can preserve sharp interfaces as compared to the smoothed characteristic function methods. We verified the new method by simple advection tests and the dam-break problem. Numerical results provide evidence for the method's improved solution quality.

Keywords: Multiphase Flow, Volume of Fluid (VOF), Interface Tracking Method, Heaviside Function.

1 Introduction

The VOF (volume of fluid) type method for interface tracking may be classified into two types according to the approximation of the interface in each grid cell. The first one is the PLIC (piecewise linear interface calculation) type method [1], which assumes a linear interface (a line in two-dimensions and a plane in three-dimensions) in each grid cell. While the normal vector of the interface can easily be calculated from the gradient of the volume fraction data, determining the interface location knowing the volume fraction and the normal vector is a quite difficult problem as it involves geometric reconstructions of the interface and complex case division [2]. The second one models the interface by a slightly smoothed characteristic function which resembles the Heaviside function in each dimension [3, 4] or multi-dimensions [5]. For example, the THINC/WLIC method [3, 4] computes interface in two steps. In the first step, the characteristic function is approximated by the one-dimensional hyperbolic tangent function. In the second step, the interface in multi-dimensions is reconstructed by a weighting function. Recently, the method [5] of applying a multi-dimensional hyperbolic tangent function has been devised. The integration of the characteristic function over the grid cell or the upwind region to determine the volume fluxes can no longer be analytically carried out. A rather complicated approach of combining a one-dimensional analytical integration of the hyperbolic tangent function and numerical quadrature is employed.

Inspired by the MTHINC [5] method, we were seeking for an analytically integrable smooth characteristic function in multi-dimension. We eventually found that the multidimensional Heaviside function itself is integrable in multi-dimensions, and even better than any smooth function. The new method is built up following these findings.

Section 2 describes the new method. Section 3 presents numerical results. Conclusions are made in Section 4.

2 The New Method

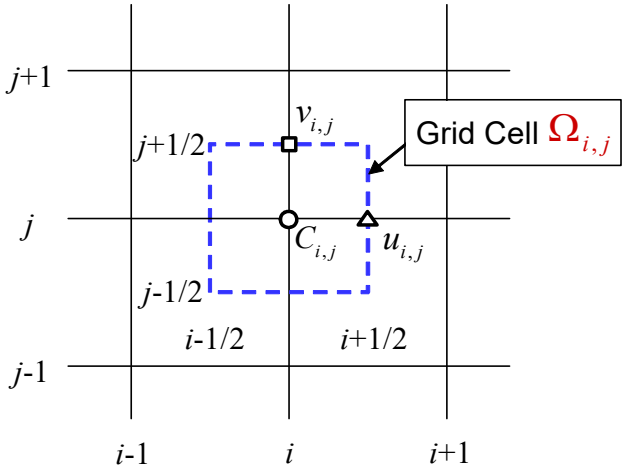

Figure 1: Grid cell.

Since extension to three dimensions is straightforward, we only consider a two-dimensional interface evolution problem in a uniform staggered grid system (Figure 1) for simplicity. In a typical VOF-type method, the interface in the grid cell $\Omega_{i,j}$ ($x_{i-1/2,j} \le x \le x_{i+1/2,j}$, $y_{i,j-1/2} \le y \le y_{i,j+1/2}$) is modeled by a characteristic function $\chi(x,y,d)$ which resembles the Heaviside function. Here d indicates the interface location. The characteristic function obeys the advection equation:

$$\frac{\partial \chi}{\partial t} + \nabla \cdot (\mathbf{u}\chi) = \chi (\nabla \cdot \mathbf{u}) \tag{1}$$

where $\mathbf{u} = (u,v)$ is the velocity vector.

Equation (1) is integrated over time $n\Delta t \le t \le (n+1)\Delta t$ and the grid cell $\Omega_{i,j}$. Denoting the cell average of χ by $C_{i,j}$, we have:

$$C_{i,j} = \frac{1}{\Omega_{i,j}} \int_{\Omega_{i,j}} \chi(x,y,d_{i,j})\, dxdy = \int_{-1/2}^{1/2} \int_{-1/2}^{1/2} \chi(\xi,\eta,d_{i,j})\, d\xi\, d\eta \tag{2}$$

where $\xi = (x - x_{i,j})/\Delta x$ and $\eta = (y - y_{i,j})/\Delta y$ are the normalized coordinates in the grid cell.

$C_{i,j}$ is updated by the following dimensional splitting scheme.

$$C^*_{i,j} = C^{(n)}_{i,j} - \frac{F^{(n)}_{x,i+1/2,j} - F^{(n)}_{x,i-1/2,j}}{\Delta x} + C^{(n)}_{i,j} \frac{u_{i,j} - u_{i-1,j}}{\Delta x} \Delta t \tag{3}$$

$$C^{(n+1)}_{i,j} = C^*_{i,j} - \frac{F^*_{y,i,j+1/2} - F^*_{y,i,j-1/2}}{\Delta y} + C^{(n)}_{i,j} \frac{v_{i,j} - v_{i,j-1}}{\Delta y} \Delta t \tag{4}$$

The volume fluxes (F_x and F_y) are calculated by the areas across the cell boundary during Δt . For the case that $u_{i,j} \ge 0$ and $v_{i,j} \ge 0$, we have

$$\begin{aligned} F_{x,i+1/2,j} &= \int_{y_{i+1/2,j-1/2}}^{y_{i+1/2,j+1/2}} \int_{x_{i+1/2,j}-u_{i,j}\Delta t}^{x_{i+1/2,j}} \chi\left(x,y,d_{i,j}\right) dxdy \\ &= \Delta x \Delta y \int_{-1/2}^{1/2} \int_{1/2-u_{i,j}\Delta t/\Delta x}^{1/2} \chi(\xi,\eta,d_{i,j})\, d\xi\, d\eta \end{aligned} \tag{5}$$

$$F_{y,i,j+1/2} = \int_{x_{i-1/2,\,j+1/2}}^{x_{i+1/2,\,j+1/2}} \int_{y_{i,j+1/2}-v_{i,j}\Delta t}^{y_{i,j+1/2}} \chi\left(x, y, d_{i,j}\right) dy dx \tag{6}$$
$$= \Delta x \Delta y \int_{-1/2}^{1/2} \int_{1/2-v_{i,j}\Delta t/\Delta y}^{1/2} \chi(\xi, \eta, d_{i,j})\, d\eta\, d\xi$$

There are three important steps to build an interface tracking method. (1) to select an analytically integrable characteristic function χ in multi-dimensions, (2) to accurately and efficiently determine $d_{i,j}$ from $C_{i,j}$, and (c) to efficiently compute the volume fluxes of χ from $d_{i,j}$.

We choose the multidimensional Heaviside Function of Equation (7) as the characteristic function.

$$\chi(\tau) = \text{Heaviside}(\tau) = \begin{cases} 1 & \tau > 0 \\ 1/2 & \tau = 0 \\ 0 & \tau < 0 \end{cases}, \quad \tau = n_x \xi + n_y \eta + d \tag{7}$$

where $(n_x, n_y) = \mathbf{n}$ stands for the unit normal vector of the interface. $\mathbf{n}$ is related to C by Eq.(8), and is subsequently required to compute d from $C_{i,j}$.

$$\mathbf{n} = \frac{\nabla C}{|\nabla C| + 10^{-7}} \tag{8}$$

The gradient of C is calculated from the following central differences to obtain $\mathbf{n}$.

$$\left.\frac{\partial C}{\partial x}\right|_{i,j} = \frac{1}{6\Delta x}\left(C_{i+1,j+1} + C_{i+1,j} + C_{i+1,j-1} - C_{i-1,j+1} - C_{i-1,j} - C_{i-1,j-1}\right) \tag{9}$$

$$\left.\frac{\partial C}{\partial y}\right|_{i,j} = \frac{1}{6\Delta y}\left(C_{i+1,j+1} + C_{i,j+1} + C_{i-1,j+1} - C_{i+1,j-1} - C_{i,j-1} - C_{i-1,j-1}\right) \tag{10}$$

Equation (7) is analytically integrable with respect to τ. The successive analytical integrations are given as follows.

$$H_1(\tau) = \int \chi(\tau) d\tau = \tau\, \chi(\tau) \tag{11}$$

$$H_2(\tau) = \int H_1(\tau) d\tau = \frac{1}{2}\tau^2\, \chi(\tau) \tag{12}$$

$$H_3(\tau) = \int H_2(\tau) d\tau = \frac{1}{6}\tau^3\, \chi(\tau) \tag{13}$$

$H_1(\tau)$, $H_2(\tau)$, and $H_3(\tau)$ are for one, two and three dimensional problems, respectively. We restrict our discussion to a two-dimensional problem.

Let us first consider the case that $n_x n_y \neq 0$ for simplicity. We have $d\xi = d\tau / n_x$ for $\eta = \text{const}$, and $d\eta = d\tau / n_y$ for $\xi = \text{const}$. The integration in Eq.(2) is analytically carried out as:

$$C_{i,j} = \int_{-1/2}^{1/2} \int_{-1/2}^{1/2} \chi(\tau)\, d\xi\, d\eta = \int_{-1/2}^{1/2} \left(\int_{-\frac{n_x}{2}+n_y\eta+d}^{\frac{n_x}{2}+n_y\eta+d} \chi(\tau) \frac{d\tau}{n_x} \right) d\eta \tag{14}$$

$$= \frac{1}{n_x}\left[\int_{-1/2}^{1/2} H_1\left(\frac{n_x}{2} + n_y\eta + d\right) d\eta - \int_{-1/2}^{1/2} H_1\left(-\frac{n_x}{2} + n_y\eta + d\right) d\eta \right]$$

$$= \frac{1}{n_x}\left[\int_{\frac{n_x}{2}-\frac{n_y}{2}+d}^{\frac{n_x}{2}+\frac{n_y}{2}+d} H_1(\tau)\frac{d\tau}{n_y} - \int_{-\frac{n_x}{2}-\frac{n_y}{2}+d}^{-\frac{n_x}{2}+\frac{n_y}{2}+d} H_1(\tau)\frac{d\tau}{n_y} \right]$$

We finally have

$$C_{i,j} = = \frac{1}{n_x n_y}\Bigg[\quad H_2\left(\frac{n_x}{2}+\frac{n_y}{2}+d\right) \quad -H_2\left(\frac{n_x}{2}-\frac{n_y}{2}+d\right) \\ -H_2\left(-\frac{n_x}{2}+\frac{n_y}{2}+d\right)+H_2\left(-\frac{n_x}{2}-\frac{n_y}{2}+d\right) \quad \Bigg] \tag{15}$$

Equation (15) provides the connection between $(C,\ n_x, n_y)_{i,j}$ and d. Given $(C,\ n_x, n_y)$, the interface location d can be easily determined from Eq.(15) by the Newton's iterative method with a few iterations (typically less than 20). Once d has been determined, the volume fluxes can also be analytically computed from Eqs. (5) and (6). For the case that either n_x or n_y equals to zero, the integration in Eq.(14) reduces to one-dimensional. Fortunately, Eq.(15) is yet applicable to such a case by just substituting the zero component with a very small value (typically $n_x = 10^{-6}$).

The proposed method is incorporated into a two-dimensional two-phase flow solver. The governing equations of the two phase flow are written as:

$$\nabla \cdot \mathbf{u} = 0 \tag{16}$$

$$\frac{\partial \mathbf{u}}{\partial t} + \mathbf{u}\cdot\nabla\mathbf{u} = -\frac{1}{\rho}\nabla p + \frac{1}{\mathrm{Re}_l}\nabla\cdot\mu\left(\nabla\mathbf{u}+\nabla\mathbf{u}^T\right) - \mathbf{e} \tag{17}$$

$$\rho = \rho_a + (\rho_l - \rho_a)C \tag{18}$$

$$\mu = \mu_a + (\mu_l - \mu_a)C \tag{19}$$

$$\mathbf{e} = \begin{pmatrix} 0 \\ 1 \end{pmatrix}, \quad \mathrm{Re}_l = \frac{\rho_l\left(\sqrt{gL}\right)L}{\mu_l} \tag{20}$$

where p is the pressure, ρ is the density and μ is the viscosity. $\mathbf{e}$ is the unite vector of upward vertical direction. The subscript *a* and *l* denote air and liquid respectively. All physical quantities except for those inside the Reynolds number (Re_l) are dimensionless.

The governing equations are discretized using staggered grids shown in Fig. 1. C, p, ρ and μ are stored at the cell center. The temporal integration is conducted as follows.

$$C^{(n)} \to C^{(n+1)} \text{ by the new method} \tag{21}$$

$$\frac{\mathbf{u}^* - \mathbf{u}^{(n)}}{\Delta t} = \frac{1}{\mathrm{Re}_l}\nabla\cdot\mu\left(\nabla\mathbf{u}^* + \nabla\mathbf{u}^{*^T}\right) \tag{22}$$

$$\frac{\mathbf{u}^{**} - \mathbf{u}^*}{\Delta t} + \mathbf{u}^{(n)}\cdot\nabla\mathbf{u}^* = 0 \tag{23}$$

$$\nabla\cdot\left(\frac{1}{\rho^{(n+1)}}\nabla p\right) = \frac{\nabla\cdot\mathbf{u}^{**}}{\Delta t} \tag{24}$$

$$\frac{\mathbf{u}^{(n+1)} - \mathbf{u}^{**}}{\Delta t} = -\frac{1}{\rho^{(n+1)}}\nabla p - \mathbf{e} \tag{25}$$

where the superscripts denote time levels.

Equation (22) is solved by a dimensional splitting semi-lagrangian method, where the advection is advanced in each dimension by the upwind third order polynomial. The pressure equation (24) and the pressure gradient in Eq.(25) are approximated by the central differences shown in Eqs. (26)-(29).

$$\left.\frac{\partial}{\partial x}\left(\frac{1}{\rho}\frac{\partial p}{\partial x}\right)\right|_{i,j} = \frac{2}{\Delta x^2}\left(\frac{p_{i+1,j}-p_{i,j}}{\rho_{i+1,j}+\rho_{i,j}} - \frac{p_{i,j}-p_{i-1,j}}{\rho_{i,j}+\rho_{i-1,j}}\right) \tag{26}$$

$$\left(\nabla\cdot\mathbf{u}^{**}\right)_{i,j} = \frac{u^{**}_{i,j}-u^{**}_{i-1,j}}{\Delta x} + \frac{v^{**}_{i,j}-v^{**}_{i,j-1}}{\Delta y} \tag{27}$$

$$\frac{u^{(n+1)}_{i,j}-u^{**}_{i,j}}{\Delta t} = -\frac{2}{\Delta x}\cdot\frac{p_{i+1,j}-p_{i,j}}{\rho^{(n+1)}_{i+1,j}+\rho^{(n+1)}_{i,j}} \tag{28}$$

$$\frac{v^{(n+1)}_{i,j}-v^{**}_{i,j}}{\Delta t} = -\frac{2}{\Delta y}\cdot\frac{p_{i,j+1}-p_{i,j}}{\rho^{(n+1)}_{i,j+1}+\rho^{(n+1)}_{i,j}} - 1 \tag{29}$$

3 Numerical results

3.1 Simple Advection Tests

We firstly present the Zalesak's solid rotation test [6] on the 200×200 uniform cells. The diameter of the slotted circle spans 60 cells and the slot width spans 12 cells. The maximum CFL number at the interface is approximately 0. 25. Figure 2 shows the computed C contours (level: 0.05, 0.5, 0.95) with the initial ones denoted by red lines. The Heaviside function approach can restrict the width of the interface within one mesh cell. The initial shape of interface is adequately preserved after one rotation, and the distortion of the interface after four rotations remains quite small.

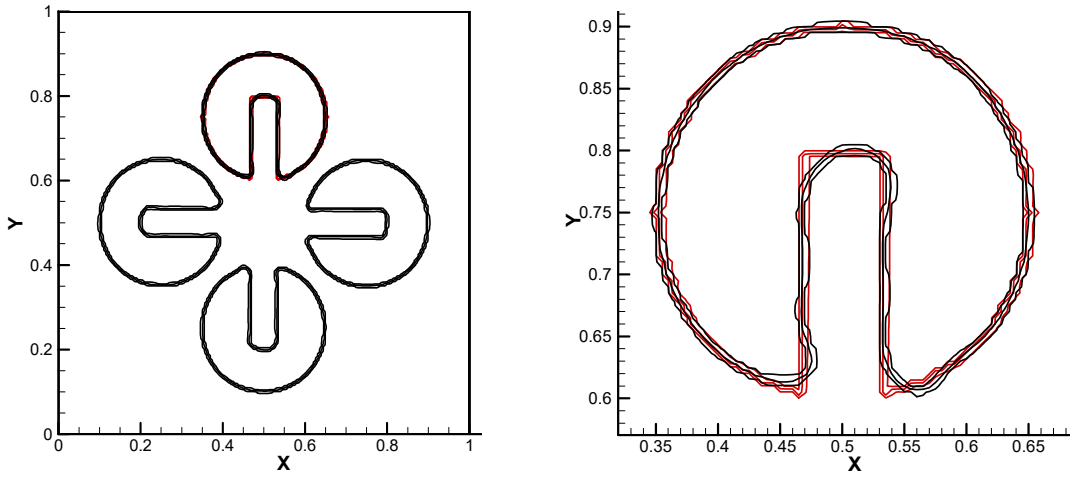

(a) During first rotation (b) After four rotations

Figure 2: Zalesak's solid rotation test on 200×200 uniform cells, initial interface (red lines), numerical solution (black lines).

We then present benchmark test with a periodically changing single vortex shearing velocity field [7] given by Eq. (30). Figure 3 shows evolution of interface on the 200×200 uniform cells. The maximum CFL number at the interface is approximately 0. 95. The C contours are again shown in three levels: 0.05, 0.5 and 0.95.

$$\begin{aligned} u &= A\sin\pi\left(x-0.5\right)\cos\pi\left(y-0.5\right) \\ v &= -A\cos\pi\left(x-0.5\right)\sin\pi\left(y-0.5\right) \\ \text{with } A &= \cos\frac{\pi t}{T} \end{aligned} \tag{30}$$

For the case of T=20, the initial shape (red cycle) of the interface is satisfactorily recovered at the half period instant regardless of the large deformation at the quarter period instant. For the case of T=30, mesh resolution becomes insufficient at the largest deformation instant that the recovered contours become partly distorted. Nevertheless, the volume error to initial volume ratio remains less than 10^{-6}.

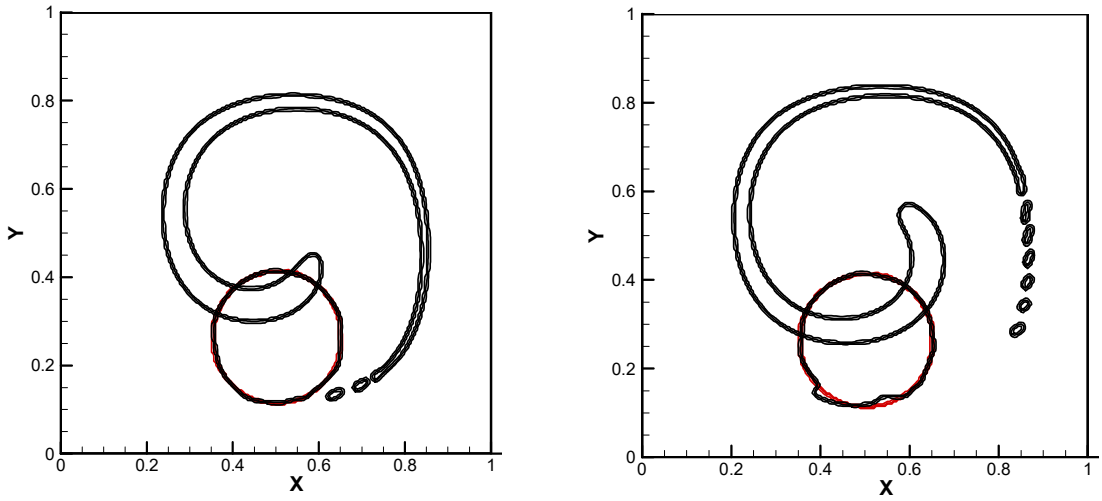

(a) T=20 (b) T=30

Figure 3: Evolution of interfaces in a periodic single vortex velocity field.

3.2 Two-dimensional Flow after a Dam Break

Dam break flow [8] serves as an important benchmark test to the free surface flow solver as it involves significant interface deformation such as overturning, breaking up and air entrapment. A rectangular water column of 1×2 in dimensionless length is initially placed at the left-bottom corner in a 4×8 open-top container, and then starts breaking down under gravity. We present numerical results on the 80×160 uniform cells, where the initial water column is covered by 40×20 cells. The dimensionless density and viscosity of water and air are given as: $\rho_l = 1$, $\rho_a = 0.0012$ and $\mu_l = 1$, $\mu_a = 0.018$. The Reynolds number and the time step length were set to $\mathrm{Re}_l = 174616$ and $\Delta t = 0.05\Delta x$, respectively. Figure 4 shows the time series of the interfaces. The areas enclosed in the red dashed lines indicate the initial and the expected final ($t \to \infty$) water areas. The water falls and runs toward the right in (a) and (b), and then hits the right wall and rises to its maximum height in (d). Although not depicted here, the right-running water front with dimensionless time are compared well with the experimental data. The water front breaks into small droplets and the air is drawn into the water in this course. The water falls in (e), runs toward the left in (f) and rises to its maximum height on the left wall in (g). After then, periodic motion with decreasing amplitude lasts a very long time.

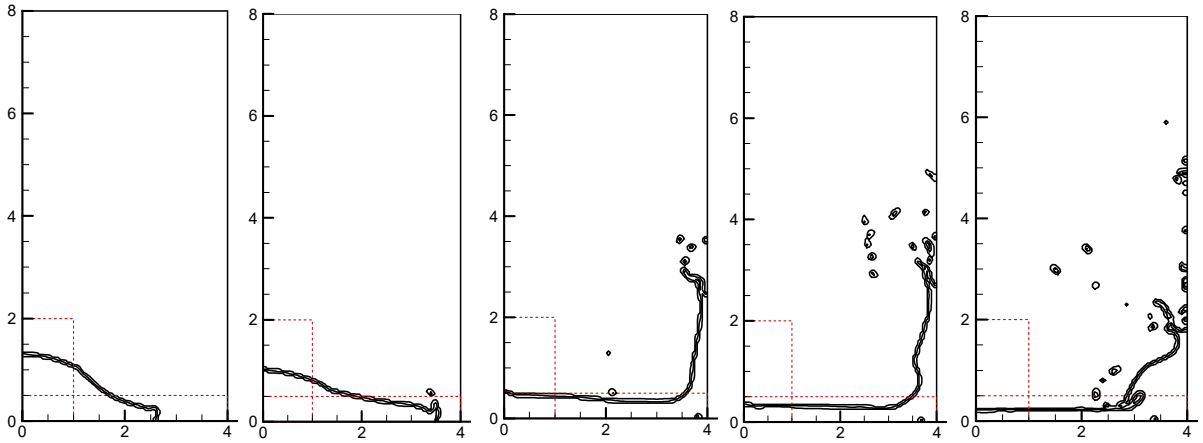

(a) t=1.50 (b) t=2.00 (c) t=3.50 (d) t=4.50 (e) t=6.00

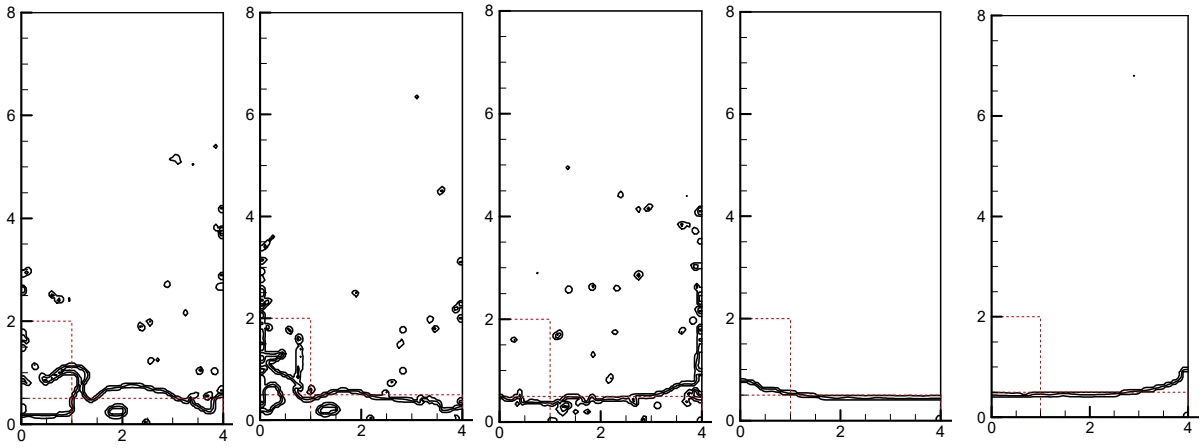

(f) t=7.75 (g) t=8.75 (h) t=14.50 (i) t=64.25 (j) t=70.00

Figure 4: Time series of interfaces of the dam break flow.

4 Conclusions

We have proposed a novel method for interface tracking using multidimensional Heaviside function. The integrations of the multidimensional Heaviside function over the grid cell and the upwind region to determine the volume fluxes are carried out analytically and explicitly. The new method bears all the benefits of the PLIC type method but does not involve geometric reconstructions of the interface. The new method is simple and efficient, can preserve sharp interfaces as compared to the smoothed characteristic function methods. Verifications conducted for simple advection tests and the dam-break problem obtained improved solution quality. Extension to three dimensions is straightforward.

Acknowledgments

This work was supported by JSPS KAKENHI Grant Number JP 17K18836.

References

[1] W.J. Rider and D.B. Kothe. Reconstructing volume tracking, J. Comput. Phys., 141: 112-152, 1998.

[2] R. Scardovelli and S. Zaleski. Analytical relations connecting linear interfaces and volume fractions in rectangular grids, J. Comput. Phys., 164: 228-237, 2000.

[3] F. Xiao, Y. Honma and T. Kono. A simple algebraic interface capturing scheme using hyperbolic tangent function, Int. J. Numer. Methods Fluid, 48: 1023–1040, 2005.

[4] K.Yokoi. Efficient implementation of THINC scheme: a simple and practical smoothed VOF algorithm, J. Comput. Phys., 226: 1985-2002, 2007.

[5] S.Ii, K.Sugiyama, S.Takeuchi, S.Takagi, Y.Matsumoto and F.Xiao. Aninterface capturing method with a continuous function: the THINC method with multi-dimensional reconstruction, J. Comput. Phys, 231: 2328–2358, 2012.

[6] S.T.Zalesak. Fully multidimensional flux-corrected transport algorithms for fluids, J. Comput. Phys. 31: 335–362, 1979.

[7] M. Rudman. Volume-tracking methods for interfacial flow calculations, Int. J. Numer. Methods Fluids 24: 671–691, 1997.

[8] J. C.Martin, W. J. Moyce. An experimental study of the collapse of liquid columns on a rigid horizontal plane, Philos. Trans. Roy. Soc. London, Ser. A, 244: 312–324, 1952.